Magnetic domain walls displacement: Automotion versus spin-transfer torque

Jean-Yves Chauleau, Raphaël Weil, André Thiaville, and Jacques Miltat
Laboratoire de Physique des Solides, CNRS UMR 8502, Univ. Paris-Sud, 91405 Orsay Cedex, France
(Received 21 October 2010; published 10 December 2010)

From the magnetization dynamics equation, a domain wall that changes structure is predicted to undergo a displacement by itself, a phenomenon called automotion. We experimentally demonstrate this effect in soft nanostrips, by transforming under spin-transfer torque a metastable asymmetric transverse wall into a vortex wall. Displacements more than three times larger than under spin-transfer torque only are measured for 1 ns pulses. The results are explained by analytical and numerical micromagnetics. Their relevance to domain-wall motion under spin-transfer torque is emphasized.

DOI: 10.1103/PhysRevB.82.214414 PACS number(s): 75.78.Fg, 72.25.Ba, 75.60.Ch

I. INTRODUCTION

The displacement of magnetic domain walls (DWs) by spin-transfer torque (STT) (Ref. 1) is presently considered as a means of control in device applications.[2] It also raises fundamental questions about the description of electronic transport in magnetic media,[3] fostering many experimental[4–7] and theoretical[8–10] studies. The former can be divided into two groups, according to the duration of current application. With long ($\approx\mu$s) pulses, average wall velocities much lower than micromagnetic expectations[11] have been first observed.[4,12] In this regime, sample heating limits the applicable current densities and wall motion occurs under a strong influence of pinning.[13] For short ($\approx$ns) pulses however, higher apparent DW velocities have been reported.[6,14–16] These have been interpreted by an easier depinning due to an additional force on the DW during the pulse risetime[17] or by a small mean distance between pinning centers.[16] The measurement of the DW *velocity* under STT is of importance because theoretical predictions relate the fundamental parameter of spin-polarized electron transport to the initial[18,19] and steady-state[9,11] DW velocities.

Under short pulse excitation, however, another type of DW motion has been documented, known as wall streaming or gyromagnetic motion in the case of NiFe films,[20] or overshoot or automotion in the case of bubble garnet films,[21] and depending on the applied field direction. The common ingredient to these situations is that certain changes in the wall structure lead to a wall displacement. This is ultimately related to the fact[22,23] that a characteristics of the wall structure (equivalent to an angle of the wall magnetization) plays the role of a linear momentum, conjugate of the wall position in Hamilton's sense. These earlier works considered extended Bloch walls where the concept of a wall angle is intuitive and where the angle changes by the displacement of so-called Bloch lines. Yet, this concept was recently shown to apply also to any type of wall in a nanostrip.[19] As a result, for the geometry of a DW in a perfect nanostrip, in the absence of any external torque (automotion), and whatever the wall type, the following equation holds:

$$\frac{d\Phi}{dt} + \frac{\alpha}{\Delta_T}\frac{dq}{dt} = 0, \tag{1}$$

where Φ is the generalized wall magnetization angle, q the (generalized) wall position, Δ_T the Thiele domain-wall width,[19] and α the Gilbert damping coefficient. This equation shows that a change in angle Φ causes a change in wall position. The numerical evaluation of the generalized angle (in fact, its time derivative) rests on a complex integral in general.[19] However, when the DW structure is planar and contains one vortex only, the angle Φ is essentially determined by the core of this vortex so that the DW displacement $[q]$ obtained by time integration (under the assumption of a constant DW width) reads

$$[q] \approx \frac{\Delta_T}{\alpha}\frac{\pi}{w}p[y_c]. \tag{2}$$

Its sign is fixed by the vortex core polarity p and by the path followed by the core (the change $[y_c]$ of its position y_c across the width w of the nanostrip). Note also that for an antivortex the result is opposite. As such changes in the wall structure have been observed after application of a current pulse,[2,5,24] it is important to experimentally evaluate the wall displacement purely due to this change. In particular, what are the signatures of this phenomenon and does automotion persist in presence of the unavoidable sample imperfections that pin the wall?

This is the object of the study described below. We apply high-resolution magnetic force microscopy (MFM) to observe wall structure and position in permalloy nanostrips, before and after sharp current pulses of nanosecond duration. Automotion is demonstrated, with a large DW displacement in a direction related to the sense of the wall angle change, rather than to current polarity. The observations are interpreted, qualitatively and quantitatively, by micromagnetics. Finally, the role played by automotion in DW dynamics under very short current pulses is discussed.

II. EXPERIMENTAL SETUP

Observations were performed in a MFM fitted with a rf connection in order to apply short current pulses. Because of space constraints, a one-port scheme was adopted, with a coplanar waveguide shorted by the sample (Fig. 1). The entire system has been characterized up to 40 GHz showing that the samples can be modeled as a resistance in parallel with a small capacitance ($\approx$0.18 pF) due to ground-signal lines proximity. Therefore, the risetime limitation is due to

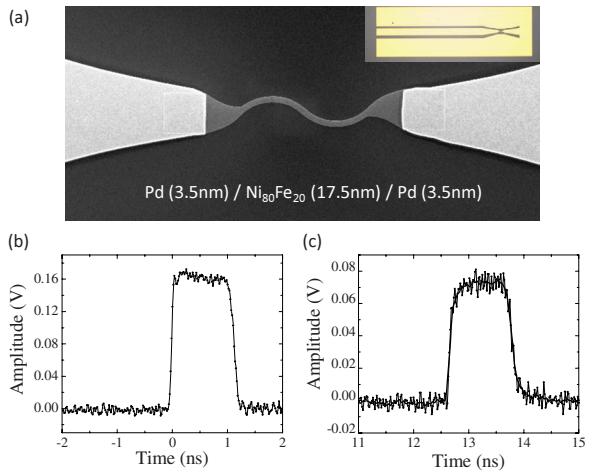

FIG. 1. (Color online) Sample and current pulses characterization. (a) Scanning electron microscopy image of one structure (inset: optical image of the entire coplanar waveguide). Oscillograms of (b) direct and (c) reflected pulses, obtained with a power divider inserted between the pulse generator and the sample. Note that a −30 dB attenuator has been added at the input of the oscilloscope.

the pulse generator (risetime: 55 ps) and attenuation in cables but is not intrinsic to the sample whose risetime is ≈8 ps. Figure 1 presents direct (b) and reflected (c) pulse profiles. The rise and falltime (10–90 %) of the reflected pulse are about 100 ps, corresponding to a characteristic time of ≈70 ps (slope at the origin). It was checked that this does not depend on the voltage amplitude so that any 1-ns-long pulse can be applied without being too much distorted. The second important parameter is the amplitude of the total current flowing into the sample. It has been measured from the power dissipated in the nanostrip. Indeed, by comparing the amplitude of the direct and the reflected pulse, one can measure the dissipated power corresponding to the current flowing into the sample (resistance). In the example presented in Figs. 1(c) and 1(d), the dissipated power was ≈0.392 W, thus leading to a total current $i \approx 22$ mA (when neglecting the attenuation in the cables <0.1 dB/m at 1 GHz). However, up to 10 GHz, the current leak into the capacitance can be neglected and eventually the total current (i) flowing into the sample can be approximated (less than 1% error) by $i=2V/(R_{dc}+50)$, with V the voltage applied on the sample and R_{dc} the resistance in the dc regime. Then, the current density has to be evaluated. Considering the sample configuration (see below), two extrema can be defined. The upper value is obtained considering that all the current flows into the NiFe layer and the lower value, considering the model of three resistances in parallel. Using the measured value for the NiFe resistivity (≈22 $\mu\Omega$ cm) and the bulk value for Pd (≈10 $\mu\Omega$ cm), we evaluated that approximately half of the current should flow into the NiFe layer. The given current densities are calculated for the intermediate value, that is, to say for 75% of the current flowing into the NiFe layer.

When performing magnetic force microscopy experiments, special care was taken for decreasing and controlling the magnetic perturbations due to the tip. First, the silicon tips were coated with a very thin $Co_{70}Cr_{30}$ (4.5 nm) layer with low coercivity, so that the tip magnetization always reverses under the DW stray field. This means that the tip-sample interaction is always attractive, as testified by a dark DW magnetic contrast. Two deleterious actions of the tip field have been observed: the DW can either be snatched when the tip approaches or dragged once the tip goes away from it. Both can be recognized in the MFM images, as a sudden appearance of DW contrast or by a staircaselike extension of this contrast along the nanostrip.[25] In such cases (less than 10% frequency), the displacement incurred was subtracted from the raw displacement. In the case where no DW image alteration by snatch-up is visible, the scatter of the DW position due to tip-sample interaction is estimated to be less than 100 nm. This upper bound is deduced from an evaluation of the tip field in the monopole approximation,[26] in comparison with the 10 Oe DW propagation field that was measured under a uniform field.

Samples were prepared from a magnetically soft $Pd(3.5)/Ni_{80}Fe_{20}(17.5)/Pd(3.5)$ multilayer (thicknesses in nanometers) patterned by e-beam lithography and lift-off into nanostrips $w=450$ nm wide and 12 μm long. A Ti(3)/Au(100) coplanar waveguide connecting the sample was fabricated in a second step. Given the samples width and thickness, vortex walls (VWs) are energetically stable.[27] Nevertheless, the DW initial state prepared by saturating the sample with a strong transverse field (≈1 kOe) is a metastable[28] asymmetric transverse wall (ATW) [Figs. 2(a) and 2(d)]. Therefore, we investigated the DW displacement when this ATW transforms into a VW. This happens most simply[29] through the injection of one vortex from the position of a precursor structure that may be called the half hedgehog vortex (1/2 HV, see Fig. 2). The vortex core then travels to the center of the nanostrip. In this process $[y_c] = \pm w/2$, so that the change in angle is large ($[\Phi]=\pm\pi/2$) and "quantized." The associated DW displacement is also large $[(q)=(\pi/2)\Delta_T/\alpha]$ and should be measurable.

Thus, the experimental protocol was as follows: for each experiment, once the created ATW is imaged, a current pulse, 1 ns long and in the range of amplitudes for STT (a few TA/m^2), is applied. The DW is then imaged again, revealing its detailed structure and the wall displacement. Note that samples have the shape of an "S" so that two different walls are simultaneously nucleated.

III. AUTOMOTION DEMONSTRATION

The DW structure transformation was realized by a current pulse through the sample (due to the STT effect), and also by a transverse field pulse, using a slightly modified sample structure.

A. Current-induced domain-wall transformation

Figure 2 shows typical results, where the ATW transformed to the stable VW structure. In every case, a DW displacement was observed, either along the direction of electron flow [Figs. 2(a) and 2(b) or in the opposite direction [Figs. 2(d) and 2(e)]. The typical displacement, ≈1 μm, would correspond to a 1 km/s effective velocity, a very large value considering the current density of 2.4 TA/m^2 (equiva-

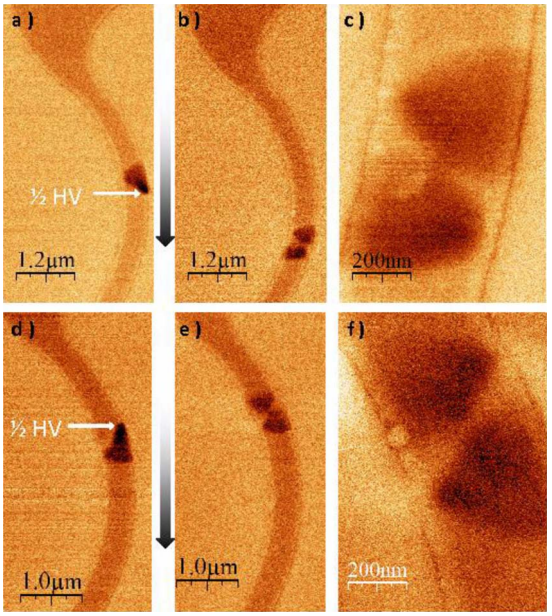

FIG. 2. (Color online) Automotion demonstrated by MFM imaging. An ATW (a) with positive asymmetry turns into a VW (b) after one current pulse (1 ns, 2.4 TA/m^2) with a displacement of 1.4 μm in the same direction as the electron flow (shaded arrow). The zoom on the core of this VW (c) shows the continuity of the dark contrast. Another ATW with negative asymmetry (d) turns into a VW (e) after one same pulse, with a displacement of 0.7 μm, now in the direction opposite to electron flow. The zoom on the vortex core (f) indicates that the bright contrast is continuous. The half hedgehog vortices (1/2 HV) are indicated in (a) and (d).

lent to a 84 m/s spin drift velocity[11]). Moreover, displacement in both directions is observed, which is not consistent with STT, even if the displacement is larger in the electron flow direction. The direction of displacement is however not random. For example, the two ATW in Fig. 2, created by the same transverse field, have the same domain and wall magnetization directions but opposite asymmetries. The asymmetry, seen as an inclination of the contrast along the nanostrip length, in either direction, appears randomly upon nucleation. We also remark that the polarities of the vortex cores in the final states are opposite (this polarity appears in the MFM images, as a continuity or an interruption of the contrast of the two wings of the VW, due to the superposition of DW and vortex core magnetic charges).

For comparison with relation [Eq. (2)], we note that the three quantities $[q]$, p, and $[y_c]$ are directly observed by MFM. For the estimation of $[y_c]$, we take the 1/2 HV to be the vortex injection position. A proof of this injection path is obtained by comparing the inclination of the stripe in between the two wings of the VW to the inclination of the ATW. As the initial y_c is 0 or w and the final $w/2$, $[y_c]$ is $\pm w/2$. Performing this check systematically, it was observed that the signs of all displacements observed under ATW to VW transformations comply with relation [Eq. (2)].

The validity of Eq. (2), independently of the DW charge (head-to-head or tail-to-tail) is demonstrated in Fig. 3. Here, two DW transformations are observed on the same image, on two ATWs with opposite magnetic charges. Note that this is

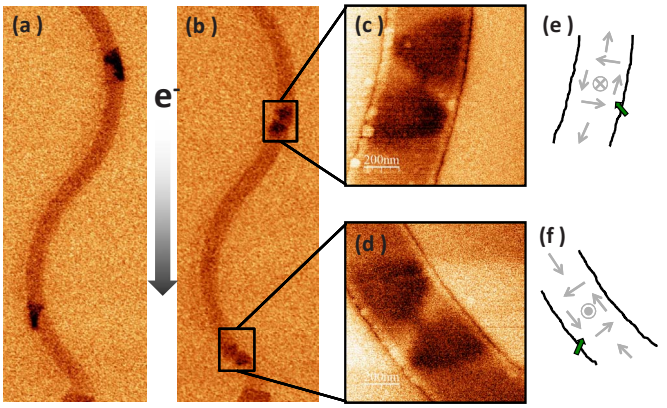

FIG. 3. (Color online) (a) MFM image of the initial magnetic state of the entire S-shaped nanostrip showing two ATWs. (b) Final magnetic state with two VWs displaced by 1.5 and 1.7 μm after transforming under a 1 ns current pulse of 3.6 TA/m^2 amplitude. [(c) and (d)] Zoom on the VWs, with schematics shown in (e) and (f), the bigger arrows indicating the vortex injection path.

a proof of the tip magnetization reversal since otherwise the walls should have appeared with opposite MFM contrasts. We observe that the two ATWs are created with 1/2 HVs located on opposite edges of the wire [Fig. 3(a)]. A 1 ns pulse of 3.6 TA/m^2 amplitude was applied. Subsequently a second MFM image was performed showing two VWs displaced by 1.5 and 1.7 μm, in the same direction [Fig. 3(b)]. Zooming onto the final states [Figs. 3(c) and 3(d)], it is seen that for both VWs the magnetic contrast is continuous between the two wings, meaning that the core polarity is the same as the DW general polarity. Therefore, since the two DWs have opposite magnetic charges, the two vortex cores have opposite polarities. This proves that for the direction of motion, the relevant parameter is the product $p[y_c]$.

B. Field-induced domain-wall transformation

Automotion depends only on the DW changes in magnetic configuration. Therefore, the type of excitation used to trigger the transformation is not a relevant parameter of the effect. As a proof, Fig. 4 presents the case of ATWs transformed into VWs by a transverse magnetic field pulse. In that case, S-shaped nanostrips with a $Pd(3.5)/Ni_{80}Fe_{20}(17.5)/SiO(10)/Al(30)/Pd(3.5)$ structure have been patterned so that the current, flowing into the Al layer generates a magnetic field transverse to the NiFe layer all along the wire.

Two ATWs with opposite asymmetries are created using the same procedure as before [Figs. 4(a) and 4(c)]. Then a 1-ns-long current pulse was applied, generating a pulsed transverse field parallel to the ATW wall magnetization ($\approx$45 mT). Subsequently, MFM images of the final state are recorded [Figs. 4(b) and 4(d)]. As expected, the DWs have turned into VWs and undergone displacements in both directions [1.76 μm in Fig. 4(b) and 1.5 μm in Fig. 4(d)]. In that case, the absolute sign of the displacement does not mean anything since no current is flowing into the magnetic layer. However the correlation between the ATW asymmetry and

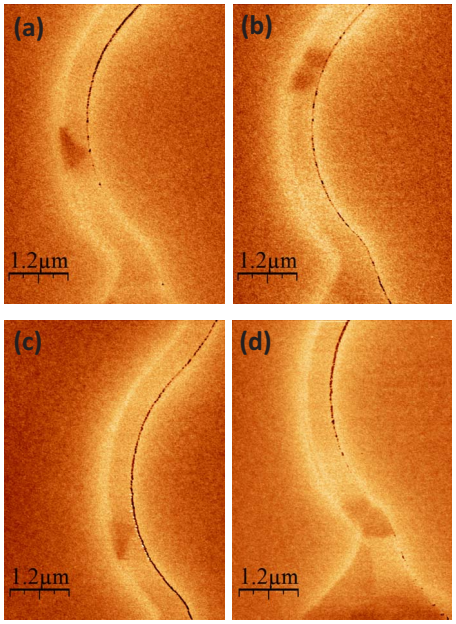

FIG. 4. (Color online) MFM images of ATWs with opposite inclination [(a) and (c)] transformed into VWs [(b) and (d)] after application of a 45 mT, 1 ns transverse magnetic field pulse.

the direction of motion is still observed. Note that, because of the thick Al layer, the core polarity could not be observed due to the resolution decrease at large tip-sample distance. These experiments demonstrate that automotion is an intrinsic phenomenon of the domain-wall dynamics.

IV. COMPARISON TO SIMULATIONS

The experiments shown above are in perfect qualitative agreement with the behavior expected for automotion. The magnitude of the displacements is now discussed. The measurements, on eight different samples with slightly varying widths $w=450-500$ nm, for different current directions and ATW asymmetries, are gathered in Fig. 5. Both positive (along the electron flow) and negative DW displacements are observed, the sign correlating with the ATW asymmetry. The displacements prove very different from those expected for a pure STT effect (shown by the solid line and discussed later). On the other hand, the calculated Thiele DW width being $\Delta_T=26$ nm for a 450×17.5 nm^2 nanostrip,[19] the analytical model predicts a displacement $(\pi/2)\Delta_T/\alpha=2.04$ μm for a damping parameter $\alpha=0.02$. This value is slightly larger than the largest displacements measured.

In order to reach a better understanding of the current-induced transformation, numerical micromagnetic computations were performed, using a homemade code[30] adapted to the infinite nanostrip geometry with a moving calculation box centered on the DW. Parameters were: current polarization $P=0.5$, nonadiabatic STT coefficient $\beta=0.08$, damping constant $\alpha=0.02$, and mesh size $3.68\times3.68\times17.5$ nm^3. The Oersted field created by the current was included. The numerically computed displacements are reported in Fig. 5. The computed minimum current density for DW transformation is 2.3 TA/m^2, and was found to be even larger for lower β,

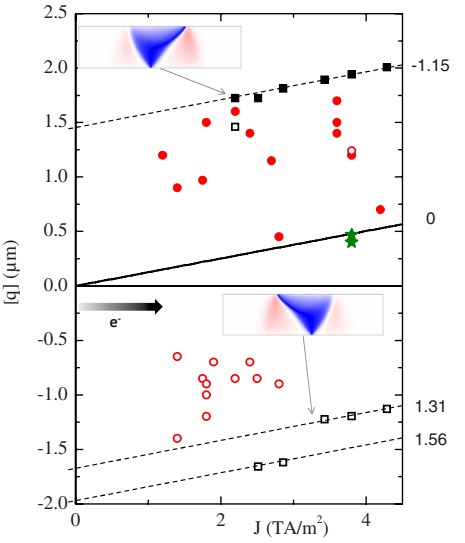

FIG. 5. (Color online) Compilation of DW displacements $[q]$ measured after ATW to VW transformations on different samples, as a function of the current density. The electron flow defines the positive axis along the nanostrip. Filled (open) circles denote positive (respectively, negative) asymmetry of the initial ATW, see the inset images (colored according to the transverse magnetization component). Squares show the micromagnetic simulation results. The solid line shows the computed pure STT displacement, to which experimental data (stars) for a VW, without transformation, have been superposed. Dashed lines link points with similar calculated $[\Phi]$, whose values are indicated on the right.

or when neglecting the Oersted field. This value is larger than the experimental threshold. However, the calculations are performed for a perfect nanostrip with no defect of any kind, especially at the edges where the vortex is injected. Besides, no temperature effect has been taken into account, which should also assist core nucleation. Thus, the obtained order-of-magnitude agreement for a perfect nanostrip is already quite good.

The calculations also show the clear correlation of displacement sign with ATW asymmetry as observed in experiments. Regarding magnitudes, one observes that the largest experimental DW displacements are close to calculations, using the effective value $\alpha=0.02$.[31] This effective value has been recognized as appropriate for DW dynamics in NiFe either by comparing field driven motion to calculations[32] or by numerically studying the effect of disorder on DW dynamics.[33] Smaller experimental displacements are ascribed to sample imperfections pinning the DW.

In addition, the calculations reveal that displacements increase with current density with a slope similar to the STT contribution. However, the data form groups with different zero-current extrapolated displacements, only the largest reaching the analytical value. This shows that the ATW transformation is in fact complex. Indeed, calculations show that vortex cores sometimes reverse polarity, this mostly happening shortly after vortex injection, when the driving force toward the nanostrip center causes large vortex core velocities. In such cases, the $[q]$ contributions of all cores have to be added (with a minus sign for antivortices), leading to reduced and sometimes reversed displacements as well as to reduced values of $[\Phi]$ (see Fig. 5).

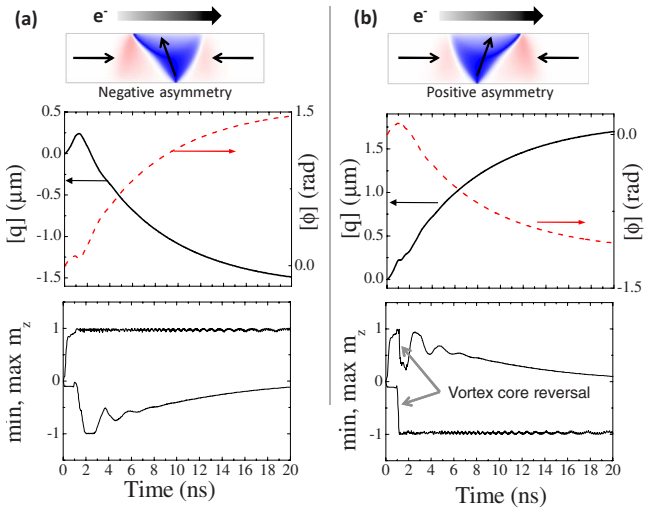

FIG. 6. (Color online) Numerical micromagnetic calculation, for an ATW with (a) positive and (b) negative asymmetry, of the effect of a 1 ns, 2.86 TA/m^2 current pulse. The wall displacement and change in generalized wall angle are plotted, as well as the maximum values for the out-of-plane magnetization component m_z.

Figure 6 details the numerical results for the situation of Fig. 2. The ATWs with opposite asymmetries finally move in opposite directions, and magnetization snapshots show that vortices of opposite polarities finally appear, even if identical vortices are initially injected at the 1/2 HV positions.[25] Indeed, for both asymmetries, the injected cores have the polarity imposed by STT. Yet, whereas for the negative asymmetry the core polarity remains unchanged until the end of core motion, for the positive asymmetry the vortex core undergoes a reversal right after its injection [Fig. 6(b), bottom]. The whole behavior is captured by the maximum and minimum values of the out-of-plane magnetization component m_z (Fig. 6). Indeed, the fact that they finally reach 1 and −1, respectively, proves that cores with opposite polarities are present into the nanostrip by end of the transformation. Note that the displacements extend over 20 ns, which corresponds to the large relaxation time of the VW (about 7 ns according to Ref. 19).

Finally, some exceptions in the correlation between the ATW asymmetry and the wall displacement are observed in experiments, as well as in micromagnetic simulations (Fig. 5). The latter show that these exceptions are due to unexpected vortex core reversals. This is what happened in the case of the negative asymmetry ATW under the current pulse of 2.2 TA/m^2. However, the sign of the end displacement is always related to the final vortex core polarity, as reversal occurs early, when vortex core velocity is large.[34]

V. STT AND AUTOMOTION

In the previous sections, the ability for a DW to move under automotion, in a real sample, has been demonstrated. Now, we discuss the role played by automotion in a regular STT displacement (without DW transformation). An experimental comparison of the displacements under DW structure transformation and under pure STT is presented in Fig. 7. An

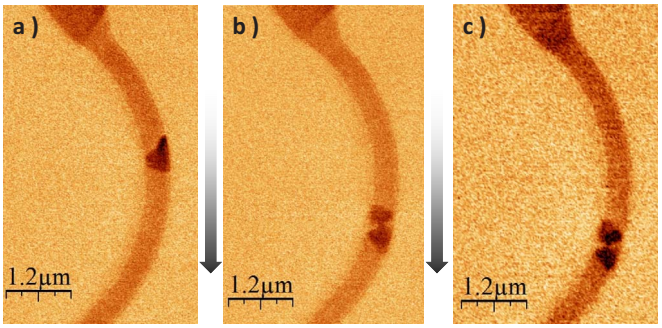

FIG. 7. (Color online) Comparison of automotion and STT-induced DW displacements. An ATW (a) turns into a VW (b) after one current pulse (1 ns, 3.8 TA/m^2) with a displacement of 1.25 μm in the same direction as the STT action. This VW displaces under STT by 400 nm (c) after another identical pulse.

ATW is nucleated (a) and then transformed into a VW by a 1 ns long current pulse of 3.8 TA/m^2 amplitude. The DW has moved by 1.2 μm downstream. Subsequently, this VW is pushed under STT by 400 nm using the very same current pulse, without any transformation. Therefore, for the short pulse used here (1 ns), the displacement due to automotion by transformation clearly dominates.

Micromagnetic calculations for different values of β have been performed for a VW submitted to a 1 ns current pulse of 3.8 TA/m^2 amplitude (Fig. 8). Both the generalized wall position q and angle Φ are shown. The angle Φ increases or decreases (depending on β) during the pulse and then goes back to zero so that no transformation occurs. Contrarily to automotion by transformation where the displacement is quantized (strictly if no vortex core switching occurs), this pure STT displacement depends on J, β, and pulse length. Note also that the measured value of the VW displacement is consistent with the value β=0.08.

Taking a closer look at those calculations, the first point to note is that for any value of β, the VW displacement extends over 20 ns (just like in the case of a transformation, see Fig. 6). By the end of the current pulse (1 ns), the VW has moved by the same distance ($\approx$133 nm) whatever β. This is due to the fact that the pulse duration is much smaller than the characteristic time of the VW (7.1 ns) so that it moves at its initial velocity v_{ini},[19]

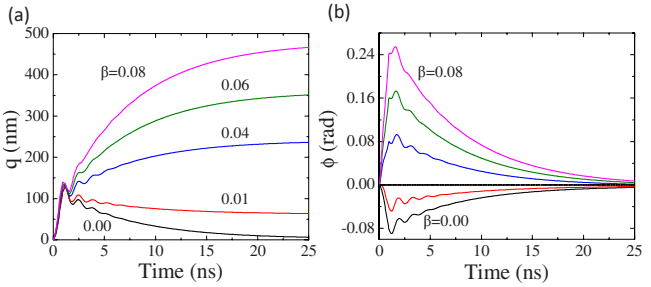

FIG. 8. (Color online) Micromagnetic simulations for a VW under a pulsed current of 1 ns and 3.8 TA/m^2 amplitude (u =133 m/s) for different values of β (α=0.02). The graphs show (a) the wall position q and (b) the generalized wall angle Φ.

$$v_{ini} = \frac{1+\beta\alpha}{1+\alpha^2} u \approx u, \tag{3}$$

as proved by the single slope seen during the current pulse. The rest of the displacement occurs while the vortex core relaxes toward the center. In other words, this part of the VW motion is performed in the automotion regime. Indeed, during the current pulse, the VW stores some linear momentum (generalized wall angle) since the vortex core is displaced from the center of the wire. This angle variation can be evaluated in the case of short pulses (compared to the VW structure relaxation time) as[19]

$$[\Phi]_{STT} = \frac{\beta-\alpha}{1+\alpha^2}\frac{1}{\Delta_T}\int u(t)dt. \tag{4}$$

So, at $t=1$ ns, the total generalized angle stored in the case of $\beta=0.08$, $\Delta_T=26$ nm is $[\Phi]=0.276$ rad, equivalent to a vortex core transversely displaced by 35 nm [note that the direction of variation is imposed by the sign of $\beta-\alpha$, Fig. 8(b)]. At the end of the current pulse, the vortex core relaxes toward the center and therefore undergoes an angle variation of 0.276 rad which leads to a displacement of $[q]=359$ nm. Added to the one obtained by pure STT, this leads to a final displacement of 492 nm. Therefore the total displacement $[q]$ has two contributions, a pure STT term and the automotion contribution

$$[q] = \frac{1+\beta\alpha}{1+\alpha^2}\cdot\int u(t)dt + \frac{\Delta_T}{\alpha}[\Phi]_{STT}. \tag{5}$$

Considering the expression (4) for the total angle variation, we obtain for the final displacement a very simple expression

$$[q] = \left(\frac{\beta}{\alpha}\right)\int u(t)dt. \tag{6}$$

This means that the displacement is the same as that expected from the steady-state regime, even if the DW has been clearly excited in the transient regime. This relation explains the straight line displaying pure STT motion added onto Fig. 5.

The derivation of Eq. (6) shows that, if automotion is somehow blocked, the VW displacement would be the same as if $\beta=\alpha$. This may provide an explanation to a number of experiments where this conclusion was reached. For example, automotion blocking could happen if the vortex core is pinned (a phenomenon directly observed in one case[5]). Note also that core pinning can occur more easily during the automotion phase since the amplitude of the relaxation force decreases exponentially with time, becoming eventually smaller than the forces linked to the shape of the current pulse.[17] Another observation to be made from these simulations is that the *real* DW velocity is never greater than u. This is of importance for device applications.

The previous discussion assumes that no relaxation occurs during the current pulse, i.e., it applies to pulses shorter than the relaxation time of the DW structure. During longer pulses (Fig. 9), the DW velocity gradually deviates from the spin drift velocity u toward the steady-state value $(\beta/\alpha)u$, as shown by the value of the displacement at current pulse end

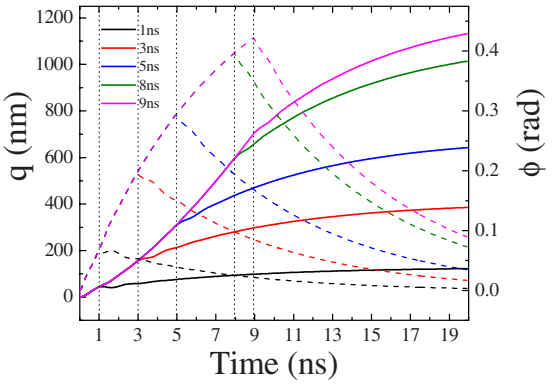

FIG. 9. (Color online) Micromagnetic calculations of a VW moving under a current pulse ($u=35$ m/s) of increasing duration, shown by the vertical lines. Both the displacement (solid curves) and the generalized wall angle (dashed curves) are plotted.

(Fig. 9), and the angle variation also deviates from Eq. (4). Nevertheless, the final extrapolated value still conforms to Eq. (6). This is directly obtained from the recalculation of Eq. (1) under STT that reads

$$\frac{d\Phi}{dt} + \frac{\alpha}{\Delta_T}\frac{dq}{dt} = \frac{\beta u}{\Delta_T}. \tag{7}$$

In the case of no transformation ($[\Phi]=0$), and neglecting the change in Δ_T, one obtains Eq. (6) by time integration.

VI. CONCLUSION

It has been experimentally demonstrated that DW automotion during a structure transformation gives rise, in real samples, to measurable displacements. A signature of the effect is the direct relation with the change in generalized wall angle, as checked by high-resolution MFM imaging. The situation chosen for this demonstration was that of a metastable ATW, frequently encountered in experiments, but the conclusions are general: a DW transformation, whatever its cause (field, current, etc.) that modifies the generalized wall angle Φ, leads to an intrinsic and large (for small damping) DW displacement. We thus propose that, once the damping constant relevant for DW dynamics is known, the magnitude of the displacement by automotion could be taken as a measure of sample quality.

When a DW transformation occurs, automotion dominates as soon as the duration of excitation is short compared to the relaxation time of the DW structure: the linear momentum bestowed to the DW when it starts transforming is very large as Φ is far from equilibrium, and it is damped over the DW structure relaxation time. In particular, the resulting displacement is of a different nature, and much larger than that due to the pulse risetime effect,[17] derived in the small Φ approximation that does not take into account the possibility of a transformation. Indeed, for the short pulses (compared to the relaxation time of the DW structure) applied here, the force due to the pulse risetime effect is close to a δ' function, that causes no DW motion.

Automotion may impact the measurements of DW displacement under pulsed excitation (field or spin-polarized

current). This is especially true for experiments in which a new DW is created prior to the application of each pulse: if this DW is not in the stable state, a transformation with a large Φ angle change is likely to occur, resulting in a DW displacement as large as what has been measured here. This may explain the apparent "better mobility" under STT of a transformed DW. In order to avoid such artifact, the absence of DW structure transformation should be checked by imaging. Alternatively, in the case where the same transformation (i.e., change in Φ) occurs for several current values, the automotion can be subtracted by linear extrapolation, as shown in Fig. 5 by the dashed lines. Moreover, even without any transformation, we have shown that an important part of the DW displacement under short current pulses is performed in the automotion regime, possibly leading to an apparent $\beta = \alpha$. We conclude that, unless $[\Phi]$ be precisely evaluated, apparent velocities may be meaningless for quantitatively evaluating the spin-transfer torque terms.

Finally, although this study has been performed on samples with a planar magnetization, the same physical arguments apply to samples with perpendicular magnetization. In that case however, as the DW widths are markedly smaller due to the presence of anisotropy, the observation of the wall structure is notoriously more difficult.

ACKNOWLEDGMENTS

This work was supported by the ANR (DYNAWALL project, Grant No. ANR-07-NANO-034). We thank M. Aprili, J. Gabelli, H. Hurdequint, and T. Devolder for their kind assistance.

[1] L. Berger, J. Appl. Phys. **55**, 1954 (1984).
[2] S. Parkin, M. Hayashi, and L. Thomas, Science **320**, 190 (2008).
[3] Y. Tserkovnyak, A. Brataas, and G. Bauer, J. Magn. Magn. Mater. **320**, 1282 (2008).
[4] A. Yamaguchi, T. Ono, S. Nasu, K. Miyake, K. Mibu, and T. Shinjo, Phys. Rev. Lett. **92**, 077205 (2004).
[5] M. Kläui, P. O. Jubert, R. Allenspach, A. Bischof, J. A. C. Bland, G. Faini, U. Rüdiger, C. A. F. Vaz, L. Vila, and C. Vouille, Phys. Rev. Lett. **95**, 026601 (2005).
[6] G. Meier, M. Bolte, R. Eiselt, B. Krüger, D.-H. Kim, and P. Fischer, Phys. Rev. Lett. **98**, 187202 (2007).
[7] V. Vlaminck and M. Bailleul, Science **322**, 410 (2008).
[8] Y. B. Bazaliy, B. A. Jones, and S.-C. Zhang, Phys. Rev. B **57**, R3213 (1998).
[9] S. Zhang and Z. Li, Phys. Rev. Lett. **93**, 127204 (2004).
[10] G. Tatara and H. Kohno, Phys. Rev. Lett. **92**, 086601 (2004).
[11] A. Thiaville, Y. Nakatani, J. Miltat, and Y. Suzuki, Europhys. Lett. **69**, 990 (2005).
[12] P.-O. Jubert, M. Kläui, A. Bischof, U. Rüdiger, and R. Allenspach, J. Appl. Phys. **99**, 08G523 (2006).
[13] S. Yang and J. L. Erskine, Phys. Rev. B **75**, 220403(R) (2007).
[14] M. Hayashi, L. Thomas, C. Rettner, R. Moriya, Y. B. Bazaliy, and S. S. P. Parkin, Phys. Rev. Lett. **98**, 037204 (2007).
[15] L. Heyne, J. Rhensius, A. Bisig, S. Krzyk, P. Punke, M. Kläui, L. Heyderman, L. Le Guyader, and F. Nolting, Appl. Phys. Lett. **96**, 032504 (2010).
[16] V. Uhlíř *et al.*, Phys. Rev. B **81**, 224418 (2010).
[17] L. Bocklage, B. Krüger, T. Matsuyama, M. Bolte, U. Merkt, D. Pfannkuche, and G. Meier, Phys. Rev. Lett. **103**, 197204 (2009).
[18] Z. Li and S. Zhang, Phys. Rev. Lett. **92**, 207203 (2004).
[19] A. Thiaville, Y. Nakatani, F. Piéchon, J. Miltat, and T. Ono, Eur. Phys. J. B **60**, 15 (2007).
[20] K. Stein and E. Feldtkeller, J. Appl. Phys. **38**, 4401 (1967).
[21] A. Malozemoff and J. Slonczewski, *Magnetic Domain Walls in Bubble Materials* (Academic Press, New York, 1979).
[22] A. Thiele, J. Appl. Phys. **47**, 2759 (1976).
[23] J. Slonczewski, J. Magn. Magn. Mater. **12**, 108 (1979).
[24] L. Heyne *et al.*, J. Appl. Phys. **103**, 07D928 (2008).
[25] See supplementary material at http://link.aps.org/supplemental/10.1103/PhysRevB.82.214414 for movies created from the micromagnetic simulations and additional details about MFM imaging.
[26] J. García, A. Thiaville, J. Miltat, K. Kirk, J. Chapman, and F. Alouges, Appl. Phys. Lett. **79**, 656 (2001).
[27] Y. Nakatani, A. Thiaville, and J. Miltat, J. Magn. Magn. Mater. **290-291**, 750 (2005).
[28] M. Kläui, C. Vaz, J. Bland, L. Heyderman, F. Nolting, A. Pavlovska, E. Bauer, S. Cherifi, S. Heun, and A. Locatelli, Appl. Phys. Lett. **85**, 5637 (2004).
[29] J.-Y. Lee, K.-S. Lee, S. Choi, K. Y. Guslienko, and S.-K. Kim, Phys. Rev. B **76**, 184408 (2007).
[30] J. Miltat and M. Donahue, *Handbook of Magnetism and Advanced Magnetic Materials* (Wiley, New York, 2007), Vol. 2, pp. 742–764.
[31] Note that, this effective value is larger than the damping parameter evaluated by ferromagnetic resonance on a control film, namely, α=0.008.
[32] Y. Nakatani, A. Thiaville, and J. Miltat, Nature Mater. **2**, 521 (2003).
[33] H. Min, R. D. McMichael, M. J. Donahue, J. Miltat, and M. D. Stiles, Phys. Rev. Lett. **104**, 217201 (2010).
[34] K. Yamada, S. Kasai, Y. Nakatani, K. Kobayashi, H. Kohno, A. Thiaville, and T. Ono, Nature Mater. **6**, 270 (2007).